Atmos. Chem. Phys. Discuss., 15, 10299–10340, 2015
www.atmos-chem-phys-discuss.net/15/10299/2015/
doi:10.5194/acpd-15-10299-2015

Atmospheric Chemistry and Physics Discussions

Effects of urban land expansion on the regional meteorology and air quality of Eastern China

W. Tao[1], J. Liu[1], G. A. Ban-Weiss[2], D. A. Hauglustaine[3], L. Zhang[4], Q. Zhang[5], Y. Cheng[6], Y. Yu[7], and S. Tao[1]

[1]Laboratory for Earth Surface Processes, College of Urban and Environmental Sciences, Peking University, Beijing 100871, China
[2]Sonny Astani Department of Civil and Environmental Engineering, University of Southern California, USA
[3]Laboratoire des Sciences du Climat et de l'Environnement, UMR8212, CEA-CNRS-UVSQ, Gif-sur-Yvette, France
[4]Laboratory for Climate and Ocean–Atmosphere Sciences, Department of Atmospheric and Oceanic Sciences, School of Physics, Peking University, Beijing 100871, China
[5]Center for Earth System Science, Tsinghua University, Beijing 100084, China
[6]Chinese Academy of Meteorological Sciences, Beijing, China
[7]Nanjing Municipal Environmental Monitoring Centre, Nanjing, Jiangsu 210013, China

Received: 27 January 2015 – Accepted: 18 March 2015 – Published: 8 April 2015

Correspondence to: J. Liu (jfliu@pku.edu.cn)

Published by Copernicus Publications on behalf of the European Geosciences Union.

ACPD
15, 10299–10340, 2015

Abstract

Rapid urbanization throughout Eastern China is imposing an irreversible effect on local climate and air quality. In this paper, we examine the response of a range of meteorological and air quality indicators to urbanization. Our study uses the Weather Research and Forecasting model coupled with Chemistry (WRF/Chem) to simulate the climate and air quality impacts of four hypothetical urbanization scenarios with fixed surface pollutant emissions during the month of July from 2008 to 2012. An improved integrated process rate (IPR) analysis scheme is implemented in WRF/Chem to investigate the mechanisms behind the forcing–response relationship at the process level. For all years, as urban land area expands, concentrations of CO, elemental carbon (EC), and particulate matter with aerodynamic diameter less than 2.5 microns ($PM_{2.5}$) tend to decrease near the surface (below ~ 500 m), but increase at higher altitudes (1–3 km), resulting in a reduced vertical concentration gradient. On the other hand, the O_3 burden averaged over all newly urbanized grid cells consistently increases from the surface to a height of about 4 km. Sensitivity tests show that the response of meteorology and pollutant concentrations to the spatial extent of urbanization are nearly linear near the surface, but nonlinear at higher altitudes. Over eastern China, each 10 % increase in nearby urban land coverage (NULC) on average leads to a decrease of approximately 2 % in surface concentrations for CO, EC, and $PM_{2.5}$, while for O_3 an increase of about 1 % is simulated. At 800 hPa, each 10 % increase in the square of NULC enhances air pollution concentrations by 5–10 %, depending on species. This indicates that as large tracts of new urban land emerge, the influence of urban expansion on meteorology and air pollution would be amplified. IPR results indicate that, for primary pollutants, the enhanced sink (source) caused by turbulent mixing and vertical advection in the lower (upper) atmosphere could be a key factor in changes to simulated vertical profiles. The evolution of secondary pollutants is further influenced by the upward relocation of precursors that impact gas phase chemistry for O_3 and aerosol processes for $PM_{2.5}$. Our study indicates that dense urbanization has a moderate dilution effect on surface pri-

ACPD
15, 10299–10340, 2015

mary airborne contaminants, but may intensify severe haze and ozone pollution if local emissions are not well controlled.

1 Introduction

Urbanization refers to the growth of urban populations and the vast expansion of urban areas. According to the 2011 Revision of the United Nations (UN) World Urbanization Prospects, the global proportion of the population living in urban areas is likely to increase to 68 % (about 6.2 billion) by 2050, and the urban population in less developed regions will almost double from 2.7 billion in 2011 to 5.1 billion in 2050 (UN, 2012). The environmental side-effects of urbanization, such as inadvertent climate modification (Changnon, 1992) and air quality degradation (Mage et al., 1996), remain an important research topic with societal relevance.

The radiative, thermal, hydrologic, and aerodynamic properties of urban land surfaces are distinct from those of natural surfaces (e.g., forests, grassland), resulting in unique exchange processes of energy, moisture, and momentum with the ambient atmosphere (Oke, 1987). Anthropogenic heat (Fan and Sailor, 2005), chemistry–climate feedbacks, and topography also contribute to the formation of distinct climatic conditions in urban areas. The features and intrinsic mechanisms of the "urban climate", which are characterized by multiple scales (Oke, 2006; Fisher et al., 2006) as well as heterogeneity in urban morphology and land cover properties, have been extensively studied. Comprehensive reviews of urban climatology (e.g. Arnfield, 2003; Kanda, 2007; Souch and Grimmond, 2006) have reported advances in recent decades in concepts such as the urban canopy layer (UCL) and roughness sublayer, observations, and numerical modeling. To date, four urban canopy schemes of different complexities have been developed: simple Bulk (BULK, Liu et al., 2006), Single-layer Urban Canopy Model (SLUCM, Kusaka and Kimura, 2004), Building Effect Parameterization (BEP, Martilli et al., 2002), and Building Energy Model (coupled to BEP, denoted as BEP + BEM, Salamanca et al., 2010). These have been implemented in mesoscale

ACPD
15, 10299–10340, 2015

meteorological models to simulate urban climate. The BULK scheme parameterizes the urban surface with greater heat capacity, thermal conductivity, roughness length, and lower albedo, rather than resolving the morphology of the urban canopy, and has been successfully employed in real-time weather forecasts (Liu et al., 2006). The last three schemes represent the urban geometry as street canyons with urban surfaces (i.e., walls, roofs, and roads), and the coupled mesoscale meteorological model of WRF and SLUCM reportedly has the ability to capture the features of an urban heat island (UHI) in some megacities (Miao et al., 2009; Lin et al., 2011; Cui and de Foy, 2012). However, these urban canopy schemes are limited by the difficulty of specifying a vast number of urban canopy parameters and initial conditions (Chen et al., 2011). The BULK scheme could capture the features of urban synoptic conditions (Liao et al., 2014), and is still being widely used for real-time meso-scale weather forecasting over urban areas (Salamanca et al., 2011).

In terms of urban air pollution meteorology, both large-scale weather patterns and land surface conditions, which play an important role in the development of local circulation and planetary boundary layer (PBL) depth, govern the dispersal, transformation, and eventual removal of airborne pollutants (Kallos et al., 1993). Efforts have been made to find the statistical relationships between Temporal Synoptic Index (TSI) and air pollution loadings (e.g. Greene et al., 1999), and the adverse meteorological conditions of severe air pollution episodes (e.g. Malek et al., 2006; Yegorova et al., 2011). However, the issues of how urban land-use changes impact the local meteorology, and thus the evolution of airborne contaminants, remain less understood, and are characterized by multiple scales. Air flows (from meso- to micro-scale) in different vertical layers above urban areas present different features. For instance, flows in the roughness sublayer are not subject to Monin–Obukhov similarity relationships, whereas upper flows in the inertial layer are in equilibrium with the underlying surface. Also, the background prevailing wind speed (threshold of $3\,m\,s^{-1}$) impacts the structure of the urban boundary layer (Fisher et al., 2006; Rotach et al., 2002). Furthermore, land–sea breezes can interact with UHI circulation (UHIC) to impact the ventilation conditions

ACPD
15, 10299–10340, 2015

(Yoshikado and Tsuchida, 1996; Ryu et al., 2013). However, the high non-uniformities of roughness elements in urban areas make it rather complicated to generalize the flow details from one landscape to another (Fernando et al., 2001). Urban air quality models are increasingly being incorporated into multi-scale integrated atmospheric models (Zhang et al., 2012; Chen et al., 2011; Baklanov et al., 2007).

A series of recent numerical studies have utilized mesoscale meteorological models, some of which are coupled to atmospheric chemical transport models, to investigate how urbanization-induced land-use changes influence the regional climate and air quality. These studies perform sensitivity tests with varying static geographic field inputs, with urbanization represented by increments in the urban land-cover fraction. Some expected climatic effects of urbanization, e.g., an increase in mean surface temperature and PBL height, and decrease in humidity and wind speed, have been captured (e.g. Zhang et al., 2010; Wang et al., 2012; Yang et al., 2012; Wang et al., 2013). Using MM5/CMAQ (the PSU/NCAR MM5 mesoscale meteorological model and the Community Multiscale Air Quality Model), Civerolo et al. (2007) compared the surface ozone concentrations in two land-use scenarios (year 1990 and 2050) in the metropolitan region of New York City, and found that when emissions were held constant, ozone levels increased across much of the area. However, when anthropogenic emissions were increased in proportion to the urbanization process, O_3 levels increased in outer counties of the metropolitan region, but decreased in other areas. Based on the Weather Research Forecasting model coupled with Chemistry (WRF/Chem), Wang et al. (2009) simulated two land-use scenarios (year 1990 and 2004) in the Pearl River Delta area. They concluded that urbanization (anthropogenic emissions were held constant) decreased surface NO_x and VOC (volatile organic compounds) levels, but increased surface O_3 and NO_3 radical levels. They also noted that SOA (secondary organic compounds) levels increased in some areas, while decreasing elsewhere. Using a similar method, Yu et al. (2012) found that urbanization-induced land-surface changes caused daytime CO and O_3 concentrations to increase in the Jing-Jin-Ji (JJJ) and Yangtze River Delta (YRD) areas of China. Applying the WRF/CMAQ model and

ACPD
15, 10299–10340, 2015

a process analysis technique, Ryu et al. (2013) analyzed the dominant forcing of urban land: the enhanced turbulence in the deep urban boundary layer diluted NO_x, which in turn reduced O_3 destruction in the NO_x-rich environment; furthermore, the prevailing urban breeze in the afternoon then brought O_3-rich and BVOC-rich air masses from surrounding mountainous areas to urban regions, all contributing to a high ozone episode in the Seoul metropolitan area.

To date, the characteristics and intrinsic mechanisms of the forcing exerted by urban land expansion on the atmospheric environment, including the burden of both primary and secondary pollutants, under current anthropogenic emission levels are not well understood, particularly throughout Eastern China. Recently, the Chinese government has relaxed its one-child policy to promote the long-term balanced development of the population, and has also launched an ambitious urbanization campaign. Therefore, it is expected that China will undergo continuous urban population growth and rapid urban land expansion in the coming decades. Note that land-use changes caused by new urban infrastructure are usually irreversible. If urban land expansion exerts adverse forcing on the ambient environment, mitigation strategies for climate and air quality improvement would be less easily implemented and more costly. Using WRF/Chem, a mesoscale fully coupled air quality and meteorological model, this study addresses two key questions: (1) How sensitive are the meteorological conditions and the spatial distribution of airborne contaminants to urban land expansion? (2) What are the intrinsic mechanisms and dominant processes that drive land-cover change induced changes in climate and atmospheric chemistry?

In Sect. 2, we present the methodology and describe the model used in this study. The model evaluation is provided in Sect. 3. In Sect. 4, we present the impact of urban land expansion on the distribution of key atmospheric species. In Sect. 5 we investigate the individual processes contributing to these changes in atmospheric composition. Conclusions are provided in Sect. 6.

ACPD
15, 10299–10340, 2015

2 Methodology

2.1 Model description and configuration

We use WRF/Chem v3.5 (Grell et al., 2005) to simulate meteorological fields and atmospheric chemistry under four hypothetical urban land surface expansion scenarios in July for the five years from 2008 to 2012. We focus on summertime air quality because of the high ozone and other secondary air pollution levels. The modeling framework is constructed on a single domain of 100 × 100 grid with a 10 km horizontal resolution, and covers nine provinces in eastern and central China (Fig. 1). In this study, the physical options include the Lin microphysics scheme (Lin et al., 1983), RRTM longwave radiation scheme (Mlawer et al., 1997), Goddard shortwave scheme (Kim and Wang, 2011), MM5 M-O surface layer scheme (Chen and Dudhia, 2001), YSU boundary layer scheme (Hong et al., 2006), New Grell cumulus scheme, and Unified Noah land surface model (Chen and Dudhia, 2001). The chemical options include the RADM2 chemical mechanism, MADE/SORGAM aerosol scheme, Madronich F-TUV photolysis scheme, and Megan biogenic emission scheme (Guenther et al., 2006). The 1.0°×1.0° NCEP Final Operational Global Analysis data (http://rda.ucar.edu/datasets/ds083.2/) have been processed to provide the meteorological initial conditions (IC) and boundary conditions (BC). We utilize the modified 2008 IGBP (International Geosphere Biosphere Programme) MODIS 20-category 30 s land-use data, which is available from the WRF website (http://www2.mmm.ucar.edu/wrf/users/), to represent current land cover conditions. Anthropogenic emission data are from Multi-resolution Emission Inventory for China (MEIC) developed by Tsinghua University for the year 2010, including five sectors (agriculture, industry, power plants, residential and transportation). The MEIC is a unit/technology based, bottom-up emission model that covers ~ 700 anthropogenic emission source categories in China. It is an update of the emission inventory developed by the same group (Zhang et al., 2009; Lei et al., 2011).

Predicted hourly ground level concentrations of CO, O_3, and particulate matter with aerodynamic diameter less than 2.5 microns ($PM_{2.5}$) are examined against obser-

ACPD
15, 10299–10340, 2015

vations made at five environmental monitoring sites, namely Nanjing Zhonghuamen Site (NJ_ZHM, 118.78° E, 32.01° N), Nanjing Xianlin Site (NJ_XL, 118.91° E, 32.11° N), Hangzhou Jiande Site (HZ_JD, 119.28° E, 29.46° N), Hangzhou Yuhang Site (HZ_YH, 119.99° E, 30.26° N) and Shanghai Pudong Site (SH_PD, 121.55° E, 31.22° N), as shown in Fig. 1. NJ_ZHM and NJ_XL are located in a mixed residential–educational area of Nanjing City, and the observation data (July 2012) are provided by Nanjing Municipal Environmental Monitoring Center. As NJ_ZHM and NJ_XL are located very close, and cannot be distinguished at the current model resolution, we average the observation data of these two sites and report it as NJ. Both HZ_JD and HZ_YH are located at high schools in Hangzhou City, and the relevant observation data (April 2008) are from Jiang et al. (2012). SH_PD is located in the urban center of Pudong District, Shanghai, and relevant observation data (September 2012) are from Tie et al. (2013). Extra simulations for April 2008 and September 2012 have been conducted for the purpose of model evaluation. The model performance is assessed by computing four conventional statistical metrics: the correlation coefficient (R), normalized mean bias (NMB), normalized mean error (NME), and index of agreement (I), which are defined as follows:

$$R = \frac{\sum_{i=1}^{N}(p_i - \overline{p})(o_i - \overline{o})}{\sqrt{\sum_{i=1}^{N}(p_i - \overline{p})^2 \cdot \sum_{i=1}^{N}(o_i - \overline{o})^2}} \quad (1)$$

$$\mathrm{NMB} = \frac{\sum_{i=1}^{N}(p_i - o_i)}{\sum_{i=1}^{N} o_i} \times 100\,\% \quad (2)$$

ACPD
15, 10299–10340, 2015

$$\mathrm{NME} = \frac{\sum_{i=1}^{N} |p_i - o_i|}{\sum_{i=1}^{N} o_i} \quad (3)$$

$$I = 1 - \frac{\sum_{i=1}^{N} (p_i - o_i)^2}{\sum_{i=1}^{N} (|p_i - \overline{o}| + |o_i - \overline{o}|)^2} \quad (4)$$

where p_i, o_i, and N represent model predicted data, observational data, and the number of data pairs, respectively. Equation (4) indicates that I is a positive value no greater than 1, the larger the value of I, the better the model performs, and a value of 1 indicates a perfect match between the model and observations.

2.2 Scenarios of urban land expansion

This work investigates the sensitivity of climatic conditions and atmospheric chemical fields to changes in urban land cover on a regional scale. Four idealized urban land surface expansion scenarios are designed within the WRF/Chem modeling framework by modifying certain static geographical parameters. The land-use fraction by category (denoted as LUF) describes the percentage coverage of different land-use categories within a given grid cell, and the land-use category (denoted as LUIND) indicates the grid's dominant land-use category. The BASE run uses the prescribed 2008 IGBP MODIS 20-category land-use data. The GE0.2 run converts all cells with an urban LUF of 0.2 or more to urban LUIND. The GE0.1 (urban LUF $\geq$ 0.1) and GT0 (urban LUF $>$ 0) urban expansion scenarios are constructed similarly. Note that only the dominant land-use category has been modified since the Noah land surface model considers only LUIND rather than a mosaic of multiple land-use categories with various LUF. Figure 1 shows a schematic map of the four idealized urban land expansion scenarios (i.e.,

ACPD
15, 10299–10340, 2015

BASE, GE0.2, GE0.1, and GT0). The urban land surface expands extensively over the YRD, and most newly urbanized regions aggregate around the periphery of the original urban districts. Figure S1 (in the Supplement) shows the original dominant land-use categories of newly urbanized cells in the GT0 run, as well as a contour map of terrain height in the domain of interest. Most new urban areas emerge to replace cropland, whereas few appear in mountainous areas.

2.3 Integrated process rate analysis

In Eulerian grid air quality models such as WRF/Chem and CMAQ, the numerical technique of operator splitting is used to solve the governing equations for species' concentrations. Operator splitting involves separating the continuity equation for each species into several simpler partial differential equations or ordinary differential equations consisting of one or two individual processes (Gipson, 1999). The technique of integrated process rate (IPR) analysis has been developed to track the accumulated contributions of individual physical and chemical processes to model predictions during runtime. IPR has already been fully implemented in CMAQ, and recent studies have reported its use in investigating a high ozone episode in the YRD (Li et al., 2012) and the Pearl River Delta (Wang et al., 2010), China, as well as the fate of major airborne pollutants in the southeastern US (Yang and Shiang-Yuh, 2013).

However, IPR has not yet been officially adopted in the WRF/Chem modeling framework. Jiang et al. (2012) added a simple process analysis scheme to WRF/Chem to calculate the contribution of photochemical and physical processes to O_3 formation. In this paper, we extend this work by implementing an improved online IPR scheme in WRF/Chem to track contributions from 10 processes, namely horizontal and vertical advection (ADVH and ADVZ), emissions (EMISS), dry deposition (DRYDEP), turbulent diffusion (DIFF), convection (CONV), gas phase chemistry (CHEM), cloud chemistry (CLDCHEM), aerosol processes (AERCHEM), and wet scavenging (WETSCAV). The calculation of dry deposition is based on resistance models for gaseous species (Wesely, 1989) and particles (Ackermann et al., 1998). Note Zhang and He (2014) recently

ACPD
15, 10299–10340, 2015

developed a new algorithm that linked dry deposition of particles with canopies via leaf area index (LAI), which is not included in the version of WRF/Chem used in this study. Cloud chemistry refers to aqueous-phase processes in different types of clouds, and aerosol processes refer to microphysical nucleation, condensation, and coagulation. Convective scavenging refers to in-cloud rainout within wet convective updrafts, whereas wet scavenging refers to below-cloud washout during large-scale precipitation. In the modal aerosol scheme MADE/SORGAM (Ackermann et al., 1998; Schell et al., 2001), $PM_{2.5}$ comprises Aitken and accumulation mode particles of sulfate, nitrate, ammonium, organic carbon (including SOA) and black carbon. The process contribution is calculated by subtracting the species burden of each cell before and after each process is simulated. In WRF/Chem, dry deposition is intermingled with vertical diffusion, so changes in the column burden during vertical mixing can be attributed to dry deposition. The IPR technique is verified by comparing the changes in species burden with the sum of contributions from the 10 processes mentioned above during each model output interval. As shown in Fig. S2, the net contribution of these 10 processes broadly matches the species concentration change.

3 Model evaluation

Figure 2 compares simulated vs. observed daily mean surface concentrations of O_3, CO, and $PM_{2.5}$ over five monitoring sites: NJ_ZHN (July 2012), NJ_XL (July 2012), SH_PD (September 2009), HZ_YH (April 2008), and HZ_JD (April 2008). The comparison indicates that WRF/Chem is capable of capturing the daily mean concentrations of surface O_3 (R = 0.66; NME = 27 %), CO (R = 0.74; NME = 41 %), and $PM_{2.5}$ (R = 0.63; NME = 29 %). Table 1 lists the statistical results for the modeled and observed hourly concentrations of O_3, CO, and $PM_{2.5}$ at above five sites. WRF/Chem generally captures the diurnal variation of surface O_3 well, with a correlation coefficient of 0.74, NMB of 6.7 %, NME of 34.1 %, and / value of 0.86. The model also reproduces the hourly surface burden of $PM_{2.5}$ and CO, with NMEs of 63.4 and 52.6 %, respectively. In addition,

ACPD
15, 10299–10340, 2015

WRF/Chem captures the monthly mean surface concentrations of O_3, CO, and $PM_{2.5}$ fairly well (although O_3 in SH is over-predicted by 17 % and CO in NJ is under-predicted by 30 %). A number of previous air quality studies have evaluated the performance of WRF/Chem in simulating a range of chemical species (e.g., $PM_{2.5}$, CO, and O_3) over China (Li et al., 2012; Tie et al., 2007, 2013), and these have reported similar results.

4 Impacts of urban land expansion on regional atmospheric environment

4.1 Urbanization-induced concentration changes

Urban land expansion significantly alters the local synoptic conditions (see Fig. S3 in the Supplement), e.g., an increase in 2 m temperature (T2) and boundary layer height (PBLH), and a decrease in 2 m relative humidity (RH2) and 10 m wind speed (W10, could be different for regions where urban land cover replaces forests). Changes in meteorology impact ambient air quality, even when anthropogenic emissions remain constant. We focus on the response of two gaseous species (i.e., CO and O_3) and two aerosol species (i.e., EC and $PM_{2.5}$). EC and CO are used to study how urban land expansion would impact the dispersion and dilution of primary pollutants. EC includes Aitken-mode EC (ECI) and accumulation-mode EC (ECJ), and the aerosol scheme simulates the aging process by converting ECI to ECJ. O_3 and $PM_{2.5}$ are used to further investigate the effects of urban land expansion on chemical reactions.

The model surface layer (Fig. 3) and 800 hPa layer (Fig. 4) are selected to study the 5 year mean concentrations in July of CO, EC, O_3, and $PM_{2.5}$ under the four urbanization scenarios. In the BASE run, high levels of surface CO (~ 850–1250 ppb), EC (~ 9–13 $\mu g\,m^{-3}$), and $PM_{2.5}$ (~ 90–130 $\mu g\,m^{-3}$) are found only in urban areas where anthropogenic emissions are high. In contrast, terrestrial O_3 (~ 24–32 ppb) is more evenly distributed on the regional scale. At 800 hPa, concentrations of CO (~ 40–70 ppb), EC (~ 0.2–0.4 $\mu g\,m^{-3}$), O_3 (~ 24–30 ppb), and $PM_{2.5}$ (~ 10–20 $\mu g\,m^{-3}$) appear much higher over the North China Plain (NCP) than in the southern domain, consis-

ACPD
15, 10299–10340, 2015

tent with the satellite-observed pollution distribution features over this domain (e.g. Liu et al., 2013). A one-tailed student t test (based on the standard error computed from hourly variability) is used to determine whether the assumed expansion of urban land causes changes in local monthly mean concentrations that are significant at the 95 % confidence level. In the surface layer, the change in dominant land-use type to urban generally induces a significant decrease in surface concentrations of CO (up to −44 %; domain-wide average of −11 %, or up to 40 ppb decrease in the GT0 run), EC (up to −80 %; domain-wide average of −21 %, or $-0.3\,\mu g\,m^{-3}$ in the GT0 run), and $PM_{2.5}$ (up to −74 %; domain-wide average of −21 %, or $-5.4\,\mu g\,m^{-3}$ in the GT0 run) in all urbanization scenarios. However, the changes in surface O_3 are generally insignificant in GE0.2. Urban land expansion leads to a moderate increase in surface O_3 (maximum of 22 %; domain-wide average of 0.3 %, equivalent to 0.1 ppb in the GT0 run) over the northern terrestrial domain in the GE0.1 and GT0 runs. At 800 hPa, the expansion of urban land significantly increases the local concentrations of CO (with a domain-wide average of 16 %, and up to 5.6 ppb in the GT0 run), EC (domain-wide average of 50 %, or $\sim 0.05\,\mu g\,m^{-3}$ in the GT0 run), O_3 (domain-wide average of 16 %, or ∼ 2.8 ppb in the GT0 run), and $PM_{2.5}$ (domain-wide average of 65 %, or $\sim 4.3\,\mu g\,m^{-3}$ in the GT0 run) in the different urbanization scenarios. The effect of urban land expansion on CO, EC, O_3 and $PM_{2.5}$ concentrations is consistent in each year, albeit with slight differences in magnitude (not shown).

4.2 Linearity of urbanization–response relationship over East China

The urbanization–response relationship is a complex function of local synoptic conditions, large-scale circulation, land surface type, the physical and chemical properties of an airborne contaminant and its emissions (e.g., release height, frequency, and amount), as well as the time scale being considered. The strength of urban land forcing (e.g., the sensitivity of an atmospheric variable to urban land expansion) can be quantitatively evaluated as the perturbation of this variable from its base condition. Fig-

ACPD
15, 10299–10340, 2015

ure 5 shows the response of the 5 year mean concentrations in July of CO, EC, O_3, and $PM_{2.5}$ to changes in domain-wide (i.e., East China) urban land coverage. At both the surface and 800 hPa, the response curves are nonlinear and the rate of domain-wide concentration changes decreases as more urban land emerges. However, as shown in Figs. 3 and 4, the concentration response is nonuniformly distributed, and becomes stronger when large tracts of new urban land appear. This indicates that the aggregation state (further discussed in the next paragraph) of newly urbanized areas would alter the strength of urban land forcing.

The forcing effect of urban land expansion on the spatial distribution of air pollutants is not usually limited to newly urbanized areas, but has a distance of extended influence. To differentiate the shape of urbanization-response curves at different locations, we use LOCAL to denote these newly urbanized cells, and ADJACENT to represent the non-urbanized cells neighboring LOCAL. We further define an aggregation parameter (Agg) for a given LOCAL cell as the number of the surrounding cells that are also LOCAL; we limit the number of surrounding grid cells for this analysis to $5 \times 5 - 1$ or 24 cells (2400 km^2). The "local" and "adjacent" forcing is defined as:

$$f_j = \frac{\sum_{i=1}^{N_j} \frac{VC_i}{VB_i}}{N_j} \quad (5)$$

where f_1 (i.e., $j = 1$) denotes local forcing (LF), N_1 is the number of domain-wide LOCAL cells, VC_i and VB_i denote the values of a certain atmospheric variable in cell i of the perturbation run and the BASE run, respectively. f_2 denotes adjacent forcing (AF) over the ADJACENT cells, and N_2 is the number of domain-wide ADJACENT cells.

Figure 6 illustrates the LF and AF induced by urban land expansion (i.e., the perturbation of 5 year mean in July concentrations of CO, EC, O_3, and $PM_{2.5}$ from the BASE situation) in all three idealized urbanization scenarios. At the surface, the relationship between LF and Agg is nearly linear. Each 10 % increase in Agg is associated with 1.6, 1.8, and 2.2 % decreases in LOCAL CO, EC, and $PM_{2.5}$ concentrations, respectively,

ACPD
15, 10299–10340, 2015

and a 1 % increase in O_3 concentrations. The AF-Agg curves are similar to those for LF-Agg, but have weaker responses. The linearity can be explained as follows: with increasing Agg, there are more LOCAL cells near a given cell, so the same number of adjacent effects are added to the given cell. At 800 hPa, changes in the contaminant burden seem to be more sensitive to the aggregation level of newly urbanized cells than at the surface, and particles seem to be more susceptible than gases. The associated urbanization-response curves become nonlinear. It can be observed that both LF and AF are linearly associated with the square of Agg, which means each 10 % increase in the square of Agg may enhance air pollution concentrations by about 5–10 % at 800 hPa, with the maximum sensitivity for $PM_{2.5}$ (12 %). This indicates that dense urbanization over East China may have a moderate dilution effect on surface air pollution, but could intensify pollutants aloft and therefore severe haze (i.e. visibility degradation) and ozone pollution if local emissions are not reduced in the future.

Besides the response of air pollutants, we found that the perturbations in July-mean PBLH, T2, and RH2 also increase linearly with Agg ($R^2 > 0.96$, shown in Fig. S4 in the Supplement). These results indicate that when large tracts of new urban land emerge, impacts of land cover change on meteorology and air pollutant concentrations can be magnified.

5 Mechanism governing the urbanization–response relationship

5.1 Process contribution to surface air quality changes

Figure 7 shows the 5 year mean in July diurnal cycles of CO, EC, O_3, and $PM_{2.5}$ surface concentrations averaged over the domain-wide LOCAL cells and the ADJACENT cells. At the surface, CO, EC, and $PM_{2.5}$ share a diurnal variation pattern in which concentrations peak at dawn (~ 05:00 LST) and reach a trough in the late afternoon (~ 16:00 LST). Concentrations over LOCAL cells are usually higher than those over the ADJACENT regions, particularly during the night. However, for O_3, the opposite

ACPD
15, 10299–10340, 2015

diurnal variation pattern can be observed, and the difference between LOCAL and ADJACENT cells is small. Urban land expansion leads to substantial changes in species concentrations, but has little effect on the shape of the diurnal cycle. As urban land expands, CO, EC, and $PM_{2.5}$ tend to evolve toward lower burden levels. In contrast, when averaged over the domain, the increment in surface O_3 concentrations during most of the day is insignificant. Though the resulting concentration changes in LOCAL and ADJACENT are quite similar for these four species, the IPR analysis suggests that the underlying mechanisms that drive the forcing–response relationship are different.

Figure 8 illustrates the 5 year mean in July diurnal cycles of IPR contributions in the BASE run and their deviations in the GT0 run over the domain-wide surface LOCAL cells and ADJACENT cells. The daytime period is chosen as 07:00–18:00 LST, with the rest of the day considered to be nighttime. In the BASE run, emissions are the dominant source of CO over the LOCAL cells, and the dominant sink is turbulent transport (daytime advection is also a contributing sink). EC follows a similar IPR pattern to CO, except that dry deposition is also a major sink, accounting for about 40 % of the total EC removal. Since this study considers constant CO and EC emissions, diurnal variability in concentrations is dominated by variations in the strength of vertical transport. During the daytime, vertical transport is strong, and CO and EC are depleted at the surface. However, during the nighttime, vertical transport becomes weaker, which allows CO and EC to accumulate. The diurnal cycle of IPR for $PM_{2.5}$ is very similar to that of EC, but aerosol processes play an important role. During the daytime, the source of $PM_{2.5}$ is dominated by surface emissions, but the sinks are quite complicated, including turbulent diffusion (~ 41 %), dry deposition (~ 36 %), and aerosol processes (~ 23 %). Note that by conducting IPR analyses within CMAQ, Yang and Shiang-Yuh (2013) found that aerosol processes depletion can act as a sink for $PM_{2.5}$. At night, the production of $PM_{2.5}$ through aerosol processes forms 22 % of the source. The IPR diurnal cycle for O_3 is quite different. During the daytime, the major sources for surface O_3 are photochemical production (~ 37 %) and turbulent transport (~ 63 %), and the sink is overwhelmingly dry deposition. At night, removal of O_3 through gas-phase

ACPD
15, 10299–10340, 2015

reactions and dry deposition accounts for 40 and 60 % of the sink, respectively. The diurnal cycles of IPR contribution over the ADJACENT cells are similar to those of LOCAL cells, except that vertical diffusion becomes a source for $PM_{2.5}$ during the daytime, compensating for the strong loss by aerosol processes and dry deposition.

In the GT0 run, as urban land expands, changes in horizontal (vertical) advection tend to increase (reduce) the surface concentration of all four species over the LOCAL cells, whereas the opposite is true for the ADJACENT cells. The associated surface wind field perturbations due to urban land expansion are shown in Fig. 9. At the surface, urban land expansion reduces the local pressure (up to 5 Pa) and forms a cyclonic anomaly. The divergence of the perturbed wind field can be calculated by a centered finite difference scheme with a one-sided difference boundary. Values of convergence up to $-6\times10^{-5}\,s^{-1}$ can be observed in most of the newly urbanized areas, similar to the results of Bornstein and Lin (2000), who concluded that UHI would induce a convergence ($\sim -10^{-5}\,s^{-1}$) zone over Atlanta. Figure 10 shows the perturbed wind field in the three vertical–longitudinal cross-sections of CS1, CS2, and CS3 mentioned in Fig. 1. The emergence of urban land induces local updrafts of $\sim 1\,cm\,s^{-1}$, which enhances the ventilation of primary pollutants to the free troposphere; adjacent downdrafts are also observed. The perturbed wind induced by urban land expansion generally forms convergence zones above the LOCAL cells and divergence zones over the ADJACENT cells (Fig. 9). UHIC is enhanced, which explains the changes in the contribution of advection.

The effects of urban land expansion are not limited to the UHIC-induced advection changes. In the surface layer, the vertical diffusion of CO is intensified over LOCAL cells (especially during the night). EC differs from CO in that the loss due to dry deposition markedly increases over the entire day, while the sink due to diffusion is only reduced during the daytime but is increased at night. The sum of dry deposition and turbulent diffusion reflects the role of vertical mixing in relocating the airborne pollutants vertically. The sink due to the vertical mixing of EC is intensified. It can be concluded that the enhanced advection and turbulent mixing in the vertical direction are the key factors

ACPD
15, 10299–10340, 2015

in reducing the surface concentrations of CO and EC. For O_3, dry deposition, vertical diffusion, and daytime photochemical production and nighttime chemical depletion are all reduced at the surface, resulting in a net weak enhancement of surface O_3 averaged over domain-wide LOCAL cells. The dry deposition of O_3 is reduced because the canopy resistance increases as vegetation is replaced by urban land; however, the dry deposition of particles is not impacted by canopy resistance, but is rather fostered by the intensified surface turbulence. Vertical diffusion is possibly hindered by convergent updrafts caused by UHIC, and the daytime photochemical production and nighttime chemical depletion are reduced because of the decreased abundance of precursors. For $PM_{2.5}$, daytime loss and nighttime production via aerosol processes are enhanced and hindered, respectively, this may be because the urbanization-induced decrease in precursor concentrations restrains gas-to-particle mass transfer. At the same time, dry deposition and vertical diffusion are also enhanced during the daytime. Therefore, the increased sink resulting from aerosol processes and dry deposition is the key factor reducing $PM_{2.5}$ concentrations at the surface. Over the ADJACENT cells, urbanization-induced outward horizontal advection contributes to the lower burden of CO, EC, and $PM_{2.5}$, and the sink term due to vertical mixing decreases.

5.2 Urbanization-induced process-level vertical profile changes

Figure 11 shows the 5 year mean in July vertical profile of the four species averaged in the domain-wide LOCAL and ADJACENT cells of the BASE and GT0 runs. In both types of cells, CO, EC, and $PM_{2.5}$ exhibit similar patterns; as urban land expands, the atmospheric burden decreases near the surface (below 1 km), but increases at higher altitudes (1–4 km). On the other hand, the concentration of O_3 increases at most heights from the surface to a height of about 4 km. Unlike near the surface, the magnitude of the concentration perturbations aloft (1–4 km) in both grids is commensurate with the atmospheric burden.

Figure 12 illustrates the vertical profile of 5 year mean in July daytime and nighttime IPR contributions for CO, EC, O_3, and $PM_{2.5}$ in the BASE and GT0 runs, averaged over

ACPD
15, 10299–10340, 2015

all LOCAL cells. Convective scavenging generally plays a minor role in removing these four species. For CO and EC, vertical mixing and advection play key roles in constraining the vertical profiles, and the net diffusion is unidirectional from the ground to higher altitudes. The extent of vertical transport during the daytime is higher than that during nighttime. The forcing of urban land expansion on the transport of primary pollutants is characterized by UHIC-induced advection changes and enhanced vertical mixing, leading to the decreased vertical concentration gradient (as shown in Fig. 11). A positive perturbation in the horizontal advection contribution and a negative perturbation in the vertical advection contribution are found in the lower atmosphere (below 500 m), whereas the opposite is true in the upper atmosphere (~ 0.5–3 km), similar to the Ekman pump. For CO and EC (only during nighttime), the enhanced sink and source due to vertical mixing in lower and upper atmosphere, respectively, could be the key reasons for changes of vertical profile, and advection appears to compensate and balance this effect. However, for EC above 1 km, as surface dry deposition is strengthened markedly in the daytime, whereas diffusion from the lower atmosphere is dampened; this is compensated by the enhanced upward advection.

For O_3, advection, vertical mixing, and gas-phase reactions all play important roles in constraining its vertical profile. Though UHIC-induced horizontal and vertical advection changes cause the IPR to shift significantly across all layers, net advection is not the key process driving the changes in the vertical O_3 profile. Near the ground level, the expansion of urban land fosters upward diffusion and hinders downward diffusion to the surface layer. O_3 production is determined by the availability of precursors, which is increased in the 1–3 km zone by the enhanced uplifting of primary pollutants. The dampened dry deposition and enhanced daytime photochemical production (at around 0.5–3 km) are responsible for a higher O_3 profile.

Besides the transport of precursors, other meteorological factors may also influence O_3 production. The bottom three plots in Fig. 10 show the distribution of chemical production (ppb h^{-1}), cloud water, and air temperature differences (GT0 minus BASE during the period 12:00–17:00 LST) in the cross-sections of CS1, CS2, and CS3 (de-

ACPD
15, 10299–10340, 2015

fined in Fig. 1). As urban land expands, air temperatures increase (up to 1.2 °C) in the lower layers (below 0.5 km), but decrease slightly above 2 km. However, photochemical production of O_3 is intensified only at altitudes higher than 2 km. This indicates that changes in air temperature may not be the principal factor determining O_3 production above the PBL. As shown in Fig. 10, the locations of newly urbanized cells exactly match the zones where photochemical production of O_3 is reduced in lower layers but cloud water content is significantly increased above 1 km. Low altitude clouds efficiently scatter shortwave radiation, thus hindering photochemical reactions below clouds; thus, urban land forcing indirectly effects the spatial distribution of O_3.

As shown in Fig. 12, aerosol chemistry, vertical mixing, and advection all contribute strongly to constraining the $PM_{2.5}$ vertical profile, with wet scavenging and cloud chemistry playing relatively minor roles. During the daytime, the contribution of aerosol chemistry is negative near the surface, but turns positive at higher altitudes. At night, the contribution of aerosol chemistry remains positive in all vertical layers. The net vertical turbulent transport is upward in the surface layer, but reverses to downward above 0.5 km. Similar to O_3, as urban land expands, changes in the vertical profiles of precursors result in enhanced aerosol production at 0.5–3 km, and enhanced loss below 0.5 km (where the downward diffusion is intensified). The perturbation of dry deposition and aerosol processes largely explains the $PM_{2.5}$ vertical profile changes.

The caveats of this study are as follows: (1) The forcing of urban land expansion on the atmospheric environment is confined to the regional scale. Feedback between mesoscale circulation and large-scale circulation, as well as inflows of airborne pollutants from outside the domain of interest, has been ignored. (2) It is important to note that emissions are assumed to remain constant during our study time period. We chose constant emissions to ensure we could tease out the effects of land-cover induced changes on air quality without confounding changes in emissions. (3) The BULK urban canopy scheme used in this work does not resolve the urban morphology, and therefore cannot further investigate how urban canopy parameters, such as the building height and anthropogenic heat, would impact the climatic conditions and

ACPD
15, 10299–10340, 2015

air quality. The urbanization–response relationship unveiled in this work could be urban scheme dependent. In future studies, we will focus on addressing these effects to better quantify the urbanization–response relationship, which could provide support to urban planning.

6 Conclusions

We have used an online coupled mesoscale meteorology-chemistry model (WRF/Chem) with BULK urban scheme embodied in Noah land surface model and an improved integrated process rate (IPR) analysis scheme to study the effects of urban land expansion in eastern China on climate and air quality during the month of July. Urban land expansion could significantly alter local synoptic conditions (e.g., increases in 2 m air temperature (T2) and boundary layer height (PBLH) and decreases in 2 m relative humidity (RH2) and 10 m wind speed (W10)). Above the newly urbanized grid cells (referred to as LOCAL cells), horizontal perturbations in wind form cyclonic convergence ($\sim 10^{-5}\,s^{-1}$) zones, and vertical perturbations in wind lead to updraft flows ($\sim 1\,cm\,s^{-1}$). This urbanization-induced circulation consequently impacts ambient air quality, even when surface emissions remain constant. For primary pollutants with strong surface emissions (e.g., CO and EC), urban land expansion causes concentrations to decrease below 500 m but increase significantly between 1 and 3 km. On the other hand, the O_3 burden averaged over LOCAL cells consistently increases from the surface to about 4 km. For $PM_{2.5}$, though its source includes both primary emissions and secondary formation, the changes in vertical profile caused by urban land expansion are consistent with those of CO and EC.

The effects of urban land expansion are not localized, but rather its influence extends to neighboring areas. In this study, the local forcing (LF) was found to be significantly larger than adjacent forcing (AF) at the surface, especially for particulate matter. The aggregation state of newly urbanized areas plays an important role in determining the strength of LF and AF. We found that perturbations of CO, EC, O_3, and $PM_{2.5}$ change

ACPD
15, 10299–10340, 2015

linearly with aggregation parameter (Agg) at the surface, and with the square of Agg at 800 hPa ($R^2 > 0.94$). In addition, the perturbations of mean July levels of PBLH, T2, and RH2 increase linearly with Agg ($R^2 > 0.96$). This result indicates that when large tracts of new urban land emerge, the effects of urban expansion on atmospheric physics and chemistry are magnified.

IPR was utilized to investigate the forcing mechanisms exerted by urban land expansion on the spatial distribution of CO, EC, O_3, and $PM_{2.5}$ over the LOCAL cells. At the surface, a common feature of all four species governed by the UHIC effect whereby horizontal advection causes increases in concentrations and vertical advection causes decreases in concentrations. Additionally, when natural vegetation was replaced by urban land, the sink term from dry deposition increased for particles but decreased for gaseous species. For primary pollutants CO and EC, enhanced advection and turbulent mixing in the vertical direction are the key factors in reducing the surface concentrations. On the other hand, for $PM_{2.5}$, increased sinks due to aerosol processes and dry deposition are the key factors in reducing surface concentrations. For O_3, the reduced dry deposition and vertical diffusion, as well as the relocation of precursors, played an important role in constraining the surface concentration, resulting in a net enhancement of the surface O_3 averaged over all LOCAL cells.

In contrast to the surface conditions, urban land expansion may induce substantial increases in air pollution at higher altitudes. The positive contribution of vertical advection and the negative contribution of horizontal advection were found to be important in the build-up of air pollution in the upper atmosphere (0.5–3 km). For primary pollutants CO and EC (only during nighttime), the enhanced uplifting caused by strengthened turbulent diffusion (induced by urban land expansion) is the key factor leading to higher burdens in the upper atmosphere. However, in daytime, diffusion of EC from the lower atmosphere is dampened due to intensified dry deposition, which partially counters the concentration increases from enhanced upward advection. However, for secondary species, O_3 and $PM_{2.5}$, the relocation of precursors accelerates daytime chemical production in the upper atmosphere, which is the key factor in the higher burden of sec-

ACPD
15, 10299–10340, 2015

ondary pollutants at a height of about 1–4 km. The urbanization–response relationship unveiled in this work could be urban scheme dependent, and more complicated urban schemes (but with higher levels of uncertainty) should be applied in future studies.

The Supplement related to this article is available online at doi:10.5194/acpd-15-10299-2015-supplement.

Acknowledgements. This work was supported by funding from the National Natural Science Foundation of China under awards 41222011, 41390240, and 41130754, the Research Project of the Chinese Ministry of Education No. 113001A, the "863" Hi-Tech R&D Program of China under Grant No. 2012AA063303, and the 111 Project (B14001).

References

Ackermann, I. J., Hass, H., Memmesheimer, M., Ebel, A., Binkowski, F. S., and Shankar, U.: Modal aerosol dynamics model for Europe: development and first applications, Atmos. Environ., 32, 2981–2999, 1998.

Arnfield, A. J.: Two decades of urban climate research: a review of turbulence, exchanges of energy and water, and the urban heat island, Int. J. Climatol., 23, 1–26, 2003.

Baklanov, A., Hänninen, O., Slørdal, L. H., Kukkonen, J., Bjergene, N., Fay, B., Finardi, S., Hoe, S. C., Jantunen, M., Karppinen, A., Rasmussen, A., Skouloudis, A., Sokhi, R. S., Sørensen, J. H., and Ødegaard, V.: Integrated systems for forecasting urban meteorology, air pollution and population exposure, Atmos. Chem. Phys., 7, 855–874, doi:10.5194/acp-7-855-2007, 2007.

Changnon, S. A.: Inadvertent weather modification in urban areas: lessons for global climate change, B. Am. Meteorol. Soc., 73, 619–627, 1992.

Chen, F. and Dudhia, J.: Coupling an advanced land surface-hydrology model with the Penn State-NCAR MM5 modeling system. Part I: Model implementation and sensitivity, Mon. Weather Rev., 129, 569–585, 2001.

Chen, F., Kusaka, H., Bornstein, R., Ching, J., Grimmond, C. S. B., Grossman-Clarke, S., Loridan, T., Manning, K. W., Martilli, A., Miao, S. G., Sailor, D., Salamanca, F. P., Taha, H.,

ACPD
15, 10299–10340, 2015

Tewari, M., Wang, X. M., Wyszogrodzki, A. A., and Zhang, C. L.: The integrated WRF/urban modelling system: development, evaluation, and applications to urban environmental problems, Int. J. Climatol., 31, 273–288, doi:10.1002/joc.2158, 2011.

Civerolo, K., Hogrefe, C., Lynn, B., Rosenthal, J., Ku, J. Y., Solecki, W., Cox, J., Small, C., Rosenzweig, C., Goldberg, R., Knowlton, K., and Kinney, P.: Estimating the effects of increased urbanization on surface meteorology and ozone concentrations in the New York City metropolitan region, Atmos. Environ., 41, 1803–1818, doi:10.1016/j.atmosenv.2006.10.076, 2007.

Cui, Y. Y. and de Foy, B.: Seasonal variations of the urban heat island at the surface and the near-surface and reductions due to urban vegetation in Mexico City, J. Appl. Meteorol. Clim., 51, 855–868, doi:10.1175/jamc-d-11-0104.1, 2012.

Fan, H. and Sailor, D. J.: Modeling the impacts of anthropogenic heating on the urban climate of Philadelphia: a comparison of implementations in two PBL schemes, Atmos. Environ., 39, 73–84, 2005.

Fernando, H., Lee, S., Anderson, J., Princevac, M., Pardyjak, E., and Grossman-Clarke, S.: Urban fluid mechanics: air circulation and contaminant dispersion in cities, Environ. Fluid Mech., 1, 107–164, 2001.

Fisher, B., Kukkonen, J., Piringer, M., Rotach, M. W., and Schatzmann, M.: Meteorology applied to urban air pollution problems: concepts from COST 715, Atmos. Chem. Phys., 6, 555–564, doi:10.5194/acp-6-555-2006, 2006.

Greene, J., Kalkstein, L., Ye, H., and Smoyer, K.: Relationships between synoptic climatology and atmospheric pollution at 4 US cities, Theor. Appl. Climatol., 62, 163–174, 1999.

Grell, G. A., Peckham, S. E., Schmitz, R., McKeen, S. A., Frost, G., Skamarock, W. C., and Eder, B.: Fully coupled "online" chemistry within the WRF model, Atmos. Environ., 39, 6957–6975, doi:10.1016/j.atmosenv.2005.04.027, 2005.

Guenther, A., Karl, T., Harley, P., Wiedinmyer, C., Palmer, P. I., and Geron, C.: Estimates of global terrestrial isoprene emissions using MEGAN (Model of Emissions of Gases and Aerosols from Nature), Atmos. Chem. Phys., 6, 3181–3210, doi:10.5194/acp-6-3181-2006, 2006.

Heilig, G. K.: World Urbanization Prospects: The 2011 Revision, United Nations, Washington, DC, 2012.

Hong, S.-Y., Noh, Y., and Dudhia, J.: A new vertical diffusion package with an explicit treatment of entrainment processes, Mon. Weather Rev., 134, 2318–2341, 2006.

ACPD
15, 10299–10340, 2015

Jiang, F., Zhou, P., Liu, Q., Wang, T., Zhuang, B., and Wang, X.: Modeling tropospheric ozone formation over East China in springtime, J. Atmos. Chem., 69, 303–319, doi:10.1007/s10874-012-9244-3, 2012.
Kallos, G., Kassomenos, P., and Pielke, R. A.: Synoptic and mesoscale weather conditions during air pollution episodes in Athens, Greece, Bound.-Lay. Meteorol., 62, 163–184, 1993.
Kanda, M.: Progress in urban meteorology: a review, J. Meteorol. Soc. Jpn., 85B, 363–383, 2007.
Kim, H.-J. and Wang, B.: Sensitivity of the WRF model simulation of the East Asian summer monsoon in 1993 to shortwave radiation schemes and ozone absorption, Asia-Pac. J. Atmos. Sci., 47, 167–180, 2011.
Kusaka, H. and Kimura, F.: Coupling a single-layer urban canopy model with a simple atmospheric model: impact on urban heat island simulation for an idealized case, J. Meteorol. Soc. Jpn., 82, 67–80, doi:10.2151/jmsj.82.67, 2004.
Lei, Y., Zhang, Q., He, K. B., and Streets, D. G.: Primary anthropogenic aerosol emission trends for China, 1990–2005, Atmos. Chem. Phys., 11, 931–954, doi:10.5194/acp-11-931-2011, 2011.
Li, L., Chen, C. H., Huang, C., Huang, H. Y., Zhang, G. F., Wang, Y. J., Wang, H. L., Lou, S. R., Qiao, L. P., Zhou, M., Chen, M. H., Chen, Y. R., Streets, D. G., Fu, J. S., and Jang, C. J.: Process analysis of regional ozone formation over the Yangtze River Delta, China using the Community Multi-scale Air Quality modeling system, Atmos. Chem. Phys., 12, 10971–10987, doi:10.5194/acp-12-10971-2012, 2012.
Liao, J., Wang, T., Wang, X., Xie, M., Jiang, Z., Huang, X., and Zhu, J.: Impacts of different urban canopy schemes in WRF/Chem on regional climate and air quality in Yangtze River Delta, China, Atmos. Res., 145, 226–243, 2014.
Lin, C. Y., Chen, W. C., Chang, P. L., and Sheng, Y. F.: Impact of the urban heat island effect on precipitation over a complex geographic environment in northern Taiwan, J. Appl. Meteorol. Clim., 50, 339–353, doi:10.1175/2010jamc2504.1, 2011.
Liu, Y., Chen, F., Warner, T., and Basara, J.: Verification of a mesoscale data-assimilation and forecasting system for the Oklahoma City area during the joint urban 2003 field project, J. Appl. Meteorol. Clim., 45, 912–929, doi:10.1175/jam2383.1, 2006.
Lin, Y.-L., Farley, R. D., and Orville, H. D.: Bulk parameterization of the snow field in a cloud model, J. Clim. Appl. Meteorol., 22, 1065–1092, 1983.

ACPD
15, 10299–10340, 2015

Liu, Y., Junfeng, L., and Shu, T.: Interannual variability of summertime aerosol optical depth over east asia during 2000–2011: a potential influence from El Nino Southern oscillation, Environ. Res. Lett., 8, 044034, doi:10.1088/1748-9326/8/4/044034, 2013.
Mage, D., Ozolins, G., Peterson, P., Webster, A., Orthofer, R., Vandeweerd, V., and Gwynne, M.: Urban air pollution in megacities of the world, Atmos. Environ., 30, 681–686, 1996.
Malek, E., Davis, T., Martin, R. S., and Silva, P. J.: Meteorological and environmental aspects of one of the worst national air pollution episodes (January 2004) in Logan, Cache Valley, Utah, USA, Atmos. Res., 79, 108–122, doi:10.1016/j.atmosres.2005.05.003, 2006.
Martilli, A., Clappier, A., and Rotach, M. W.: An urban surface exchange parameterisation for mesoscale models, Bound.-Lay. Meteorol., 104, 261–304, doi:10.1023/a:1016099921195, 2002.
Miao, S. G., Chen, F., Lemone, M. A., Tewari, M., Li, Q. C., and Wang, Y. C.: An observational and modeling study of characteristics of urban heat island and boundary layer structures in Beijing, J. Appl. Meteorol. Clim., 48, 484–501, doi:10.1175/2008jamc1909.1, 2009.
Mlawer, E. J., Taubman, S. J., Brown, P. D., Iacono, M. J., and Clough, S. A.: Radiative transfer for inhomogeneous atmospheres: RRTM, a validated correlated-k model for the longwave, J. Geophys. Res., 102, 16663–16682, 1997.
Oke, T. R.: Boundary Layer Climates, 2nd edn., Routledge, London, UK, 1987.
Oke, T. R.: Towards better scientific communication in urban climate, Theor. Appl. Climatol., 84, 179–190, 2006.
Rotach, M. W., Fisher, B., and Piringer, M.: Cost 715 workshop on urban boundary layer parameterizations, B. Am. Meteorol. Soc., 83, 1501–1504, doi:10.1175/bams-83-10-1501, 2002.
Ryu, Y.-H., Baik, J.-J., Kwak, K.-H., Kim, S., and Moon, N.: Impacts of urban land-surface forcing on ozone air quality in the Seoul metropolitan area, Atmos. Chem. Phys., 13, 2177–2194, doi:10.5194/acp-13-2177-2013, 2013.
Salamanca, F., Krpo, A., Martilli, A., and Clappier, A.: A new building energy model coupled with an urban canopy parameterization for urban climate simulations-part I. formulation, verification, and sensitivity analysis of the model, Theor. Appl. Climatol., 99, 331–344, doi:10.1007/s00704-009-0142-9, 2010.
Salamanca, F., Martilli, A., Tewari, M., and Chen, F.: A study of the urban boundary layer using different urban parameterizations and high-resolution urban canopy parameters with WRF, J. Appl. Meteorol. Clim., 50, 1107–1128, doi:10.1175/2010jamc2538.1, 2011.

ACPD
15, 10299–10340, 2015

Schell, B., Ackermann, I. J., Hass, H., Binkowski, F. S., and Ebel, A.: Modeling the formation of secondary organic aerosol within a comprehensive air quality model system, J. Geophys. Res.-Atmos., 106, 28275–28293, 2001.

Souch, C. and Grimmond, S.: Applied climatology: urban climate, Prog. Phys. Geog., 30, 270–279, 2006.

Tie, X., Madronich, S., Li, G., Ying, Z., Zhang, R., Garcia, A. R., Lee-Taylor, J., and Liu, Y.: Characterizations of chemical oxidants in Mexico City: a regional chemical dynamical model (WRF-Chem) study, Atmos. Environ., 41, 1989–2008, 2007.

Tie, X., Geng, F., Guenther, A., Cao, J., Greenberg, J., Zhang, R., Apel, E., Li, G., Weinheimer, A., Chen, J., and Cai, C.: Megacity impacts on regional ozone formation: observations and WRF-Chem modeling for the MIRAGE-Shanghai field campaign, Atmos. Chem. Phys., 13, 5655–5669, doi:10.5194/acp-13-5655-2013, 2013.

Wang, J., Feng, J., Yan, Z., Hu, Y., and Jia, G.: Nested high-resolution modeling of the impact of urbanization on regional climate in three vast urban agglomerations in China, J. Geophys. Res.-Atmos., 117, D21103, doi:10.1029/2012JD018226, 2012.

Wang, M. N., Zhang, X. Z., and Yan, X. D.: Modeling the climatic effects of urbanization in the Beijing-Tianjin-Hebei metropolitan area, Theor. Appl. Climatol., 113, 377–385, doi:10.1007/s00704-012-0790-z, 2013.

Wang, X., Wu, Z., and Liang, G.: WRF/CHEM modeling of impacts of weather conditions modified by urban expansion on secondary organic aerosol formation over Pearl River Delta, Particuology, 7, 384–391, doi:10.1016/j.partic.2009.04.007, 2009.

Wang, X., Zhang, Y., Hu, Y., Zhou, W., Lu, K., Zhong, L., Zeng, L., Shao, M., Hu, M., and Russell, A. G.: Process analysis and sensitivity study of regional ozone formation over the Pearl River Delta, China, during the PRIDE-PRD2004 campaign using the Community Multiscale Air Quality modeling system, Atmos. Chem. Phys., 10, 4423–4437, doi:10.5194/acp-10-4423-2010, 2010.

Wesely, M.: Parameterization of surface resistances to gaseous dry deposition in regional-scale numerical models, Atmos. Environ., 23, 1293–1304, 1989.

Yang, B., Zhang, Y. C., and Qian, Y.: Simulation of urban climate with high-resolution WRF model: a case study in Nanjing, China, Asia-Pac. J. Atmos. Sci., 48, 227–241, doi:10.1007/s13143-012-0023-5, 2012.

ACPD
15, 10299–10340, 2015

Yang, Z. and Shiang-Yuh, W.: Understanding of the fate of atmospheric pollutants using a process analysis tool in a 3-D regional air quality model at a fine grid scale, Atmospheric and Climate Sciences, 3, 18–30, doi:10.4236/acs.2013.31004, 2013.

Yegorova, E. A., Allen, D. J., Loughner, C. P., Pickering, K. E., and Dickerson, R. R.: Characterization of an eastern US severe air pollution episode using WRF/Chem, J. Geophys. Res.-Atmos., 116, D17306, doi:10.1029/2010jd015054, 2011.

Yoshikado, H. and Tsuchida, M.: High levels of winter air pollution under the influence of the urban heat island along the shore of Tokyo Bay, J. Appl. Meteorol., 35, 1804–1813, doi:10.1175/1520-0450(1996)035<1804:hlowap>2.0.co;2, 1996.

Yu, M., Carmichael, G. R., Zhu, T., and Cheng, Y. F.: Sensitivity of predicted pollutant levels to urbanization in China, Atmos. Environ., 60, 544–554, doi:10.1016/j.atmosenv.2012.06.075, 2012.

Zhang, L. and He, Z.: Technical Note: An empirical algorithm estimating dry deposition velocity of fine, coarse and giant particles, Atmos. Chem. Phys., 14, 3729–3737, doi:10.5194/acp-14-3729-2014, 2014.

Zhang, N., Gao, Z. Q., Wang, X. M., and Chen, Y.: Modeling the impact of urbanization on the local and regional climate in Yangtze River Delta, China, Theor. Appl. Climatol., 102, 331–342, doi:10.1007/s00704-010-0263-1, 2010.

Zhang, Q., Streets, D. G., Carmichael, G. R., He, K. B., Huo, H., Kannari, A., Klimont, Z., Park, I. S., Reddy, S., Fu, J. S., Chen, D., Duan, L., Lei, Y., Wang, L. T., and Yao, Z. L.: Asian emissions in 2006 for the NASA INTEX-B mission, Atmos. Chem. Phys., 9, 5131–5153, doi:10.5194/acp-9-5131-2009, 2009.

Zhang, Y., Karamchandani, P., Glotfelty, T., Streets, D. G., Grell, G., Nenes, A., Yu, F., and Bennartz, R.: Development and initial application of the global-through-urban weather research and forecasting model with chemistry (GU-WRF/Chem), J. Geophys. Res.-Atmos., 117, D20206, doi:10.1029/2012JD017966, 2012.

ACPD
15, 10299–10340, 2015

Table 1. Statistical results for the modeled and observed hourly concentrations over sites NJ (July 2012), SH_PD (September 2009), HZ_YH (April 2008), and HZ_JD (April 2008) for CO, O_3, and $PM_{2.5}$.

Species	Correlation coefficient	NMB (%)	NME (%)	/
CO	0.22	−22.4	52.6	0.49
O_3	0.74	6.7	34.1	0.86
$PM_{2.5}$	0.38	11.2	63.4	0.60

ACPD
15, 10299–10340, 2015

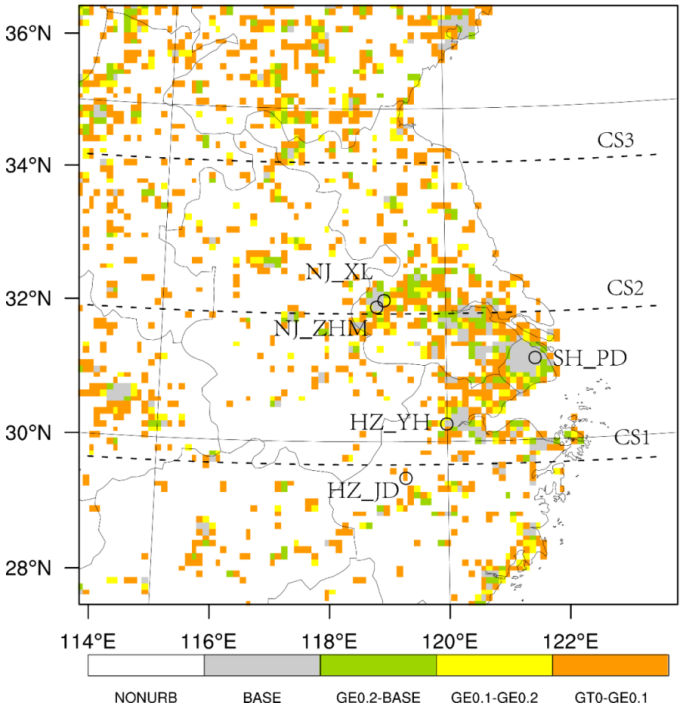

Figure 1. Schematic map of four idealized urban land expansion scenarios (i.e., BASE, GE0.2, GE0.1, and GT0). White denotes non-urban cells, and grey denotes urban cells in the BASE run. Other colors represent additional newly urbanized cells in GE0.2 (green), GE0.1 (yellow), and GT0 (orange) compared to previous urban land expansion scenarios. For example, urban cells in GE0.1 are grey, green, and yellow. Black open circles denote the five air quality monitoring sites. Black dashed lines running west–east demarcate the three vertical-zonal cross-sections CS1, CS2, and CS3.

ACPD
15, 10299–10340, 2015

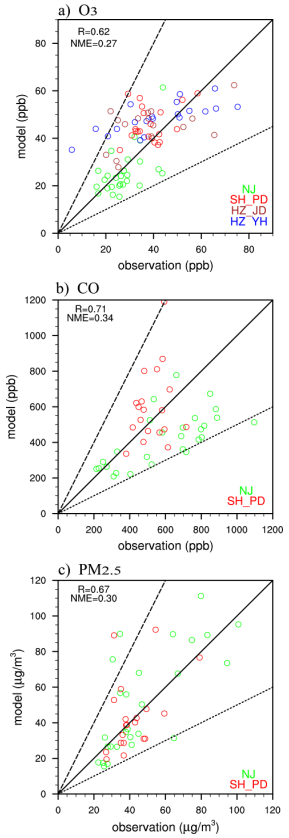

Figure 2. Modeled vs. observed daily mean surface concentrations of **(a)** O_3, **(b)** CO, and **(c)** $PM_{2.5}$ at NJ (July 2012), SH_PD (September 2009), HZ_YH (April 2008) and HZ_JD (April 2008). Solid line indicates the 1 : 1 line; dashed lines indicate the 1 : 2 and 2 : 1 lines.

ACPD
15, 10299–10340, 2015

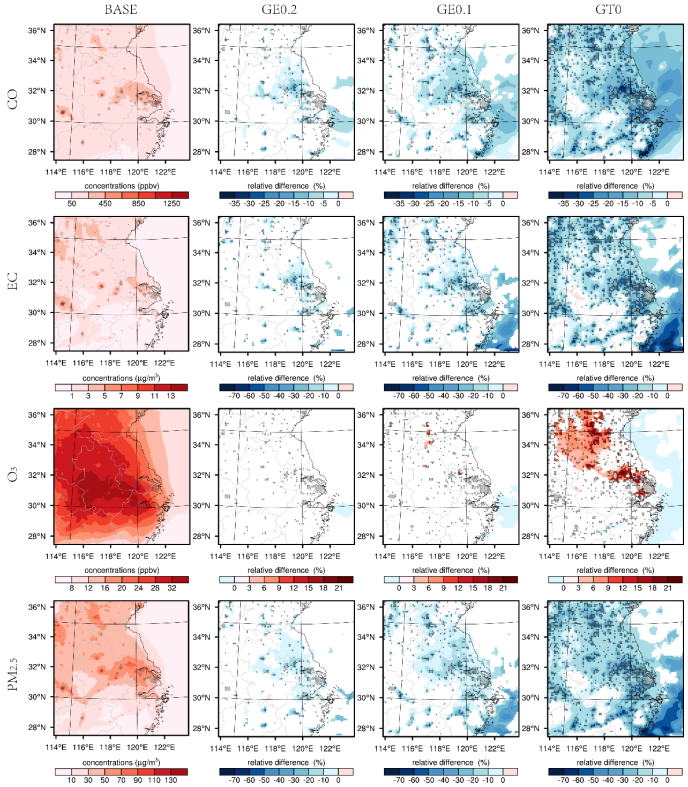

Figure 3. Five-year mean surface concentrations in July of CO, EC, O_3, and $PM_{2.5}$ in the BASE run (left), and the relative difference (only cells exceeding the 95 % significance level are shown) of each urban land expansion scenario relative to BASE (right three columns). Grey circles indicate urban areas in the BASE run; black crosses indicate newly urbanized cells in GE0.2, GE0.1, and GT0.

ACPD
15, 10299–10340, 2015

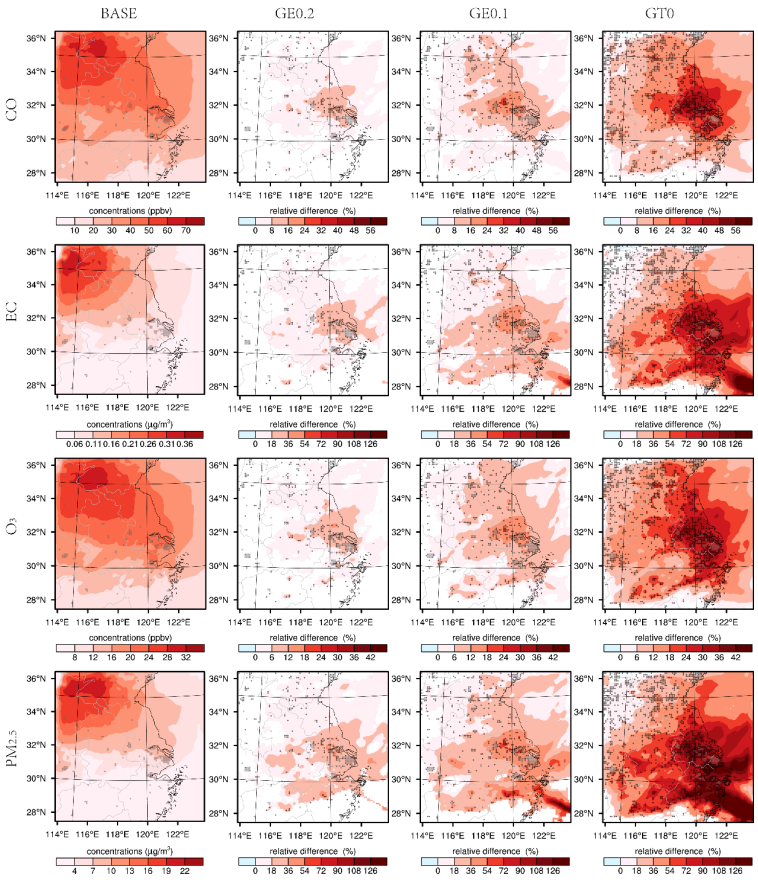

Figure 4. Same as Fig. 3, but at 800 hPa.

ACPD
15, 10299–10340, 2015

Effects of urban land expansion on the regional meteorology and air quality

W. Tao et al.

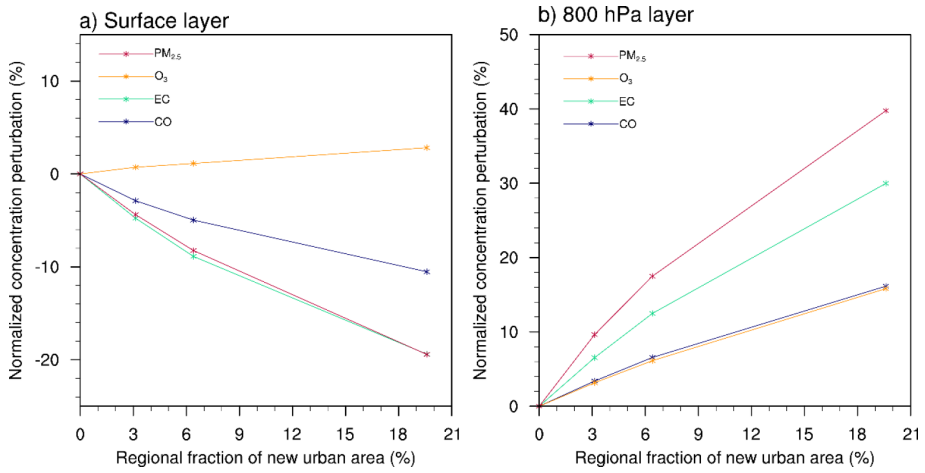

Figure 5. Normalized perturbations (relative to the BASE simulation) for three urbanization scenarios of the 5 year mean concentrations in July of CO, EC, O_3, and $PM_{2.5}$ at the **(a)** surface and **(b)** 800 hPa. Values are averaged over land for the entire domain. Corresponding domain-wide land fraction of new urban areas are 3, 6, and 20 %, respectively, relative to BASE.

ACPD
15, 10299–10340, 2015

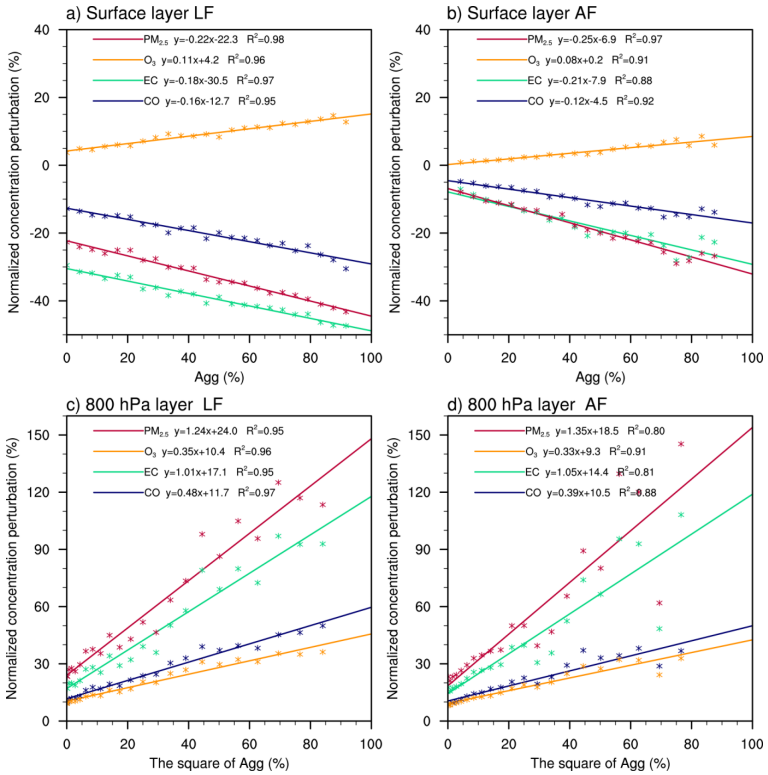

Figure 6. Relationship between normalized perturbations of 5 year mean July concentrations of CO, EC, O_3, and $PM_{2.5}$ and Agg at the surface (top), and the square of Agg at 800 hPa (bottom) for the LOCAL forcing (LF, left) and ADJACENT forcing (AF, right). Agg is defined as the occupation rate of the newly urbanized cells to the surrounding 24 ($5 \times 5 - 1$) cells. Linear regression results are also shown.

ACPD
15, 10299–10340, 2015

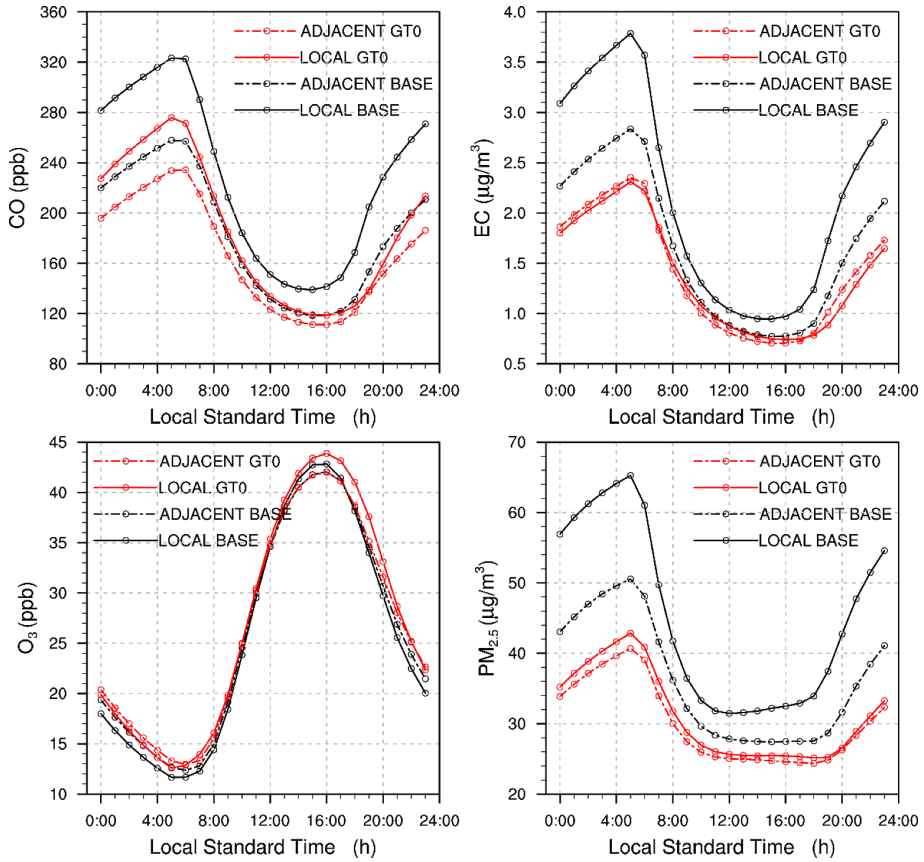

Figure 7. Simulated 5 year mean July diurnal cycle of CO, EC, O_3, and $PM_{2.5}$ at the surface, averaged over domain-wide LOCAL cells (solid lines) and ADJACENT cells (dashed lines).

ACPD
15, 10299–10340, 2015

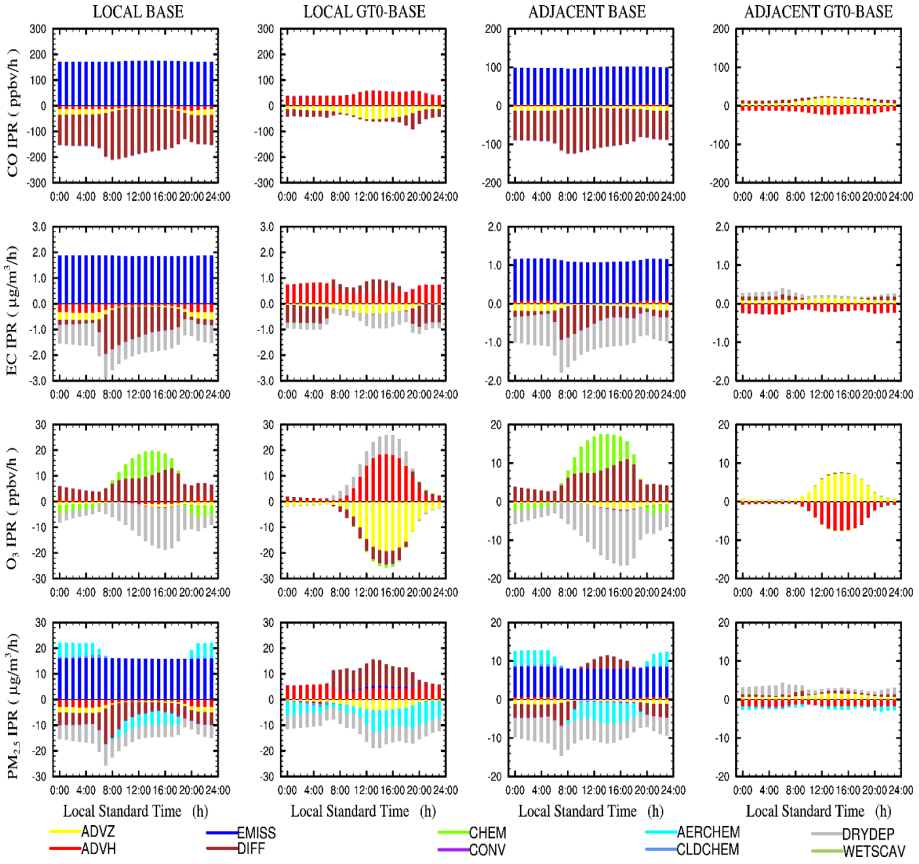

Figure 8. Five-year mean in July diurnal cycles of IPR for surface CO, EC, O_3, and $PM_{2.5}$ concentrations. Values are averaged over all LOCAL (left two columns) and ADJACENT (right two columns) cells. Results are shown for the BASE simulation and for differences between GT0 and BASE.

ACPD
15, 10299–10340, 2015

Effects of urban land expansion on the regional meteorology and air quality

W. Tao et al.

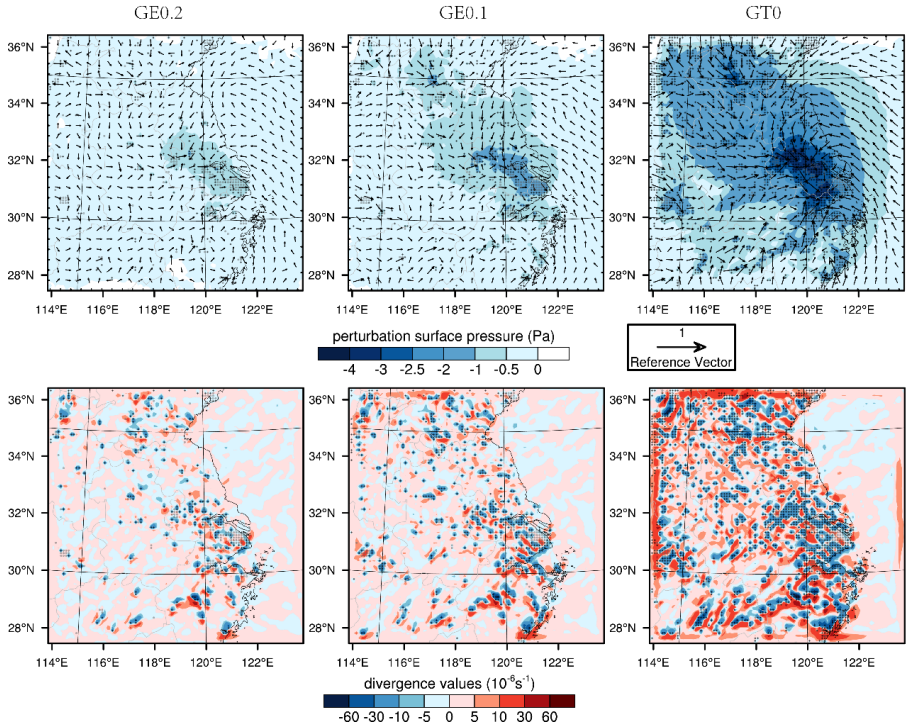

Figure 9. Five-year mean July perturbations of surface pressure and wind field (top three plots, reference velocity is 1 m s^{-1}) and the divergence of surface wind (bottom three plots) in GE0.2, GE0.1, GT0 runs. Grey circles indicate the locations of urban cells in the BASE run; black crosses indicate the locations of newly urbanized areas in GE0.2, GE0.1, and GT0 runs.

ACPD
15, 10299–10340, 2015

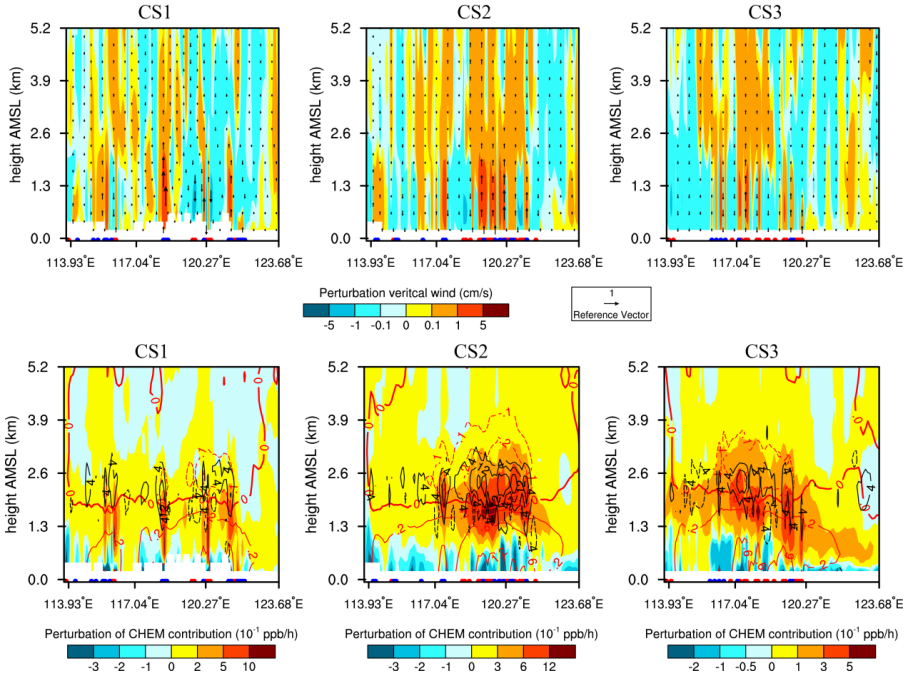

Figure 10. Distribution of 5 year mean July perturbations (GT0 minus BASE) of vertical wind velocities (top three plots, reference wind velocity is 1 cm s^{-1}), O_3 production (color, ppb h^{-1}), cloud water content (black line, mg kg^{-1}), and air temperature (red line, K) during 12:00–17:00 LST (bottom three plots) in CS1, CS2, and CS3. Red and blue dots indicate the longitudes of LOCAL cells in the GT0 run along the cross-section lines and adjacent areas, respectively.

ACPD
15, 10299–10340, 2015

Effects of urban land expansion on the regional meteorology and air quality

W. Tao et al.

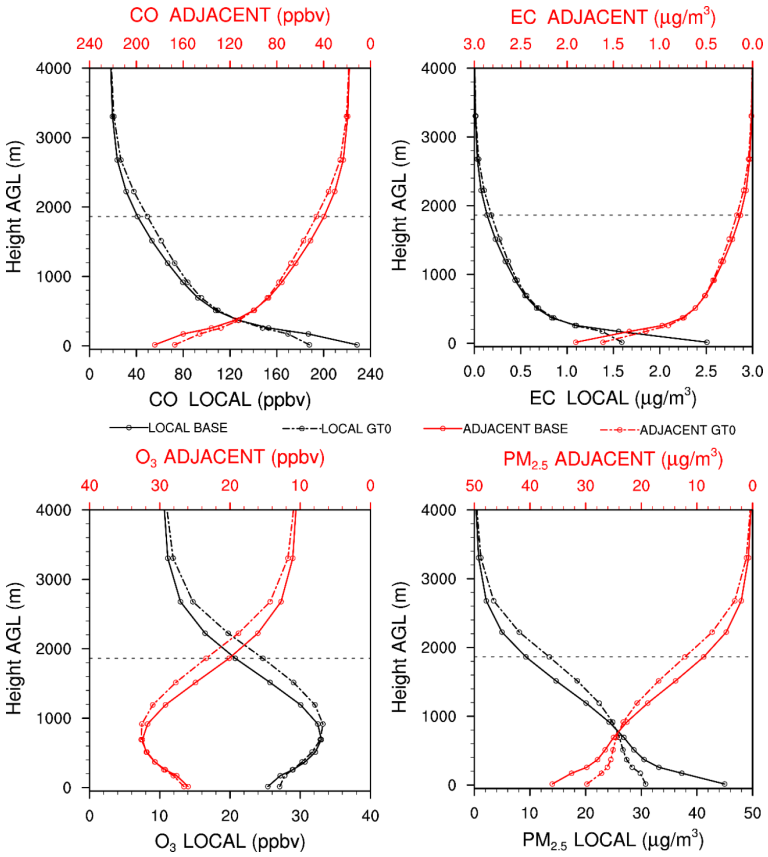

Figure 11. Five-year mean July vertical profiles of CO, EC, O_3, and $PM_{2.5}$ concentrations over the LOCAL cells (black) and ADJACENT cells (red) in the BASE (solid lines) and GT0 run (dashed lines). The horizontal dashed lines indicate the height of 800 hPa.

ACPD
15, 10299–10340, 2015

Effects of urban land expansion on the regional meteorology and air quality

W. Tao et al.

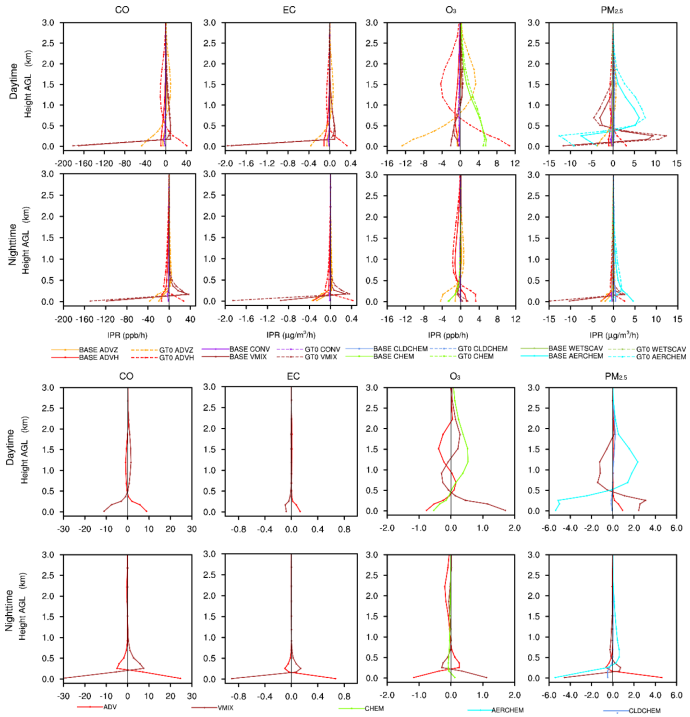

Figure 12. Five-year mean in July vertical profiles of diurnal (07:00–18:00 LST) and nocturnal (19:00–06:00 LST) IPR for CO, EC, O_3, and $PM_{2.5}$ concentrations in the BASE and GT0 run (top eight figures). The bottom eight plots show the difference in IPR between GT0 and the BASE simulation for advection (ADV), vertical mixing (VMIX), gas phase chemistry (CHEM), aerosol processes (AERCHEM), and cloud chemistry (CLDCHEM), averaged over domain-wide LOCAL cells.

ACPD
15, 10299–10340, 2015